IOPscience iopscience.iop.org

Home Search Collections Journals About Contact us My IOPscience

Conductance fluctuation theory for a mixed transport regime

This article has been downloaded from IOPscience. Please scroll down to see the full text article.

1998 J. Phys.: Condens. Matter 10 10035

(http://iopscience.iop.org/0953-8984/10/44/011)

View the table of contents for this issue, or go to the journal homepage for more

Download details:
IP Address: 171.66.16.210
The article was downloaded on 14/05/2010 at 17:46

Please note that terms and conditions apply.

J. Phys.: Condens. Matter **10** (1998) 10035–10059. Printed in the UK PII: S0953-8984(98)94767-1

Conductance fluctuation theory for a mixed transport regime

Ningjia Zhu, Hong Guo and R Harris

Department of Physics and Centre for the Physics of Materials, McGill University, Montréal, Québec, H3A 2T8 Canada

Received 2 June 1998, in final form 4 August 1998

Abstract. We analyse the non-universal conductance fluctuations for a dirty quantum wire in a transport regime where both mesoscopic and ballistic transport characteristics play a role. This 'mixed' transport regime is reached when impurities are distributed near the walls of a quantum wire, leaving the centre region ballistic. Using a diagrammatic technique, we find that the existence of a ballistic region destroys the conventional universal conductance fluctuations. The crossover behaviour of the fluctuation amplitude from the usual quasi-1D situation to that of the mixed regime is clearly revealed, and the role of various length scales identified. Our analytical predictions are confirmed by a direct numerical evaluation of the Landauer–Büttiker formula.

1. Introduction

In recent years semiconductor nanostructures have provided opportunities for investigating electrical conduction on very short length scales. In addition, a complete understanding of electronic transport in these submicron and ultra-submicron systems is indispensable for device applications. Among the many discoveries [1], one of the most interesting is the existence of *universal* conductance fluctuations (UCF) in the mesoscopic transport regime [2, 3]. In this case the conductance of a sample has a characteristic fluctuation amplitude which is independent of the details of the elastic scattering centres, of the value of the Fermi energy or of the strength of an external magnetic field. Due to an assumption of ergodicity [2], such a fluctuation amplitude also describes the sample-to-sample fluctuation which is usually more amenable to theoretical analysis. The mesoscopic transport regime is characterized by several important length scales: the elastic mean free path l, the electron phase coherence length ξ, and the sample size L; this regime is reached when $l < L \ll \xi$. On the other hand, when the sample is extremely small such that $L < l \ll \xi$, there is effectively no impurity scattering and conduction is only limited by the sample shape and by the boundary scattering. This is the so-called ballistic transport regime [1].

The mesoscopic transport regime has been observed in metallic samples where there are many elastic scattering centres such as impurities and imperfections of the crystalline structure. These scattering centres are distributed randomly and *uniformly* throughout the sample. Correspondingly, the diagrammatic technique has successfully been applied to the calculation of conductance fluctuations in this situation [2, 3]. On the other hand, many situations of potential interest for device applications have both mesoscopic and ballistic ingredients. For instance, it is known that the electron mobility in a MOSFET is substantially influenced by the quality of the Si–SiO_2 interface [4, 5, 6, 7], and parameters characterizing

0953-8984/98/4410035+25$19.50 © 1998 IOP Publishing Ltd

scattering at the rough interface can be extracted from experimental data [8]. Similarly, for a quantum MESFET [9] the roughness at the metal–semiconductor interface provides the 'impurity scattering'. Equally, as free-standing quantum wires become a reality, one must deal with the impurity scattering problem near the boundaries, as impurities tend to diffuse into the wire in this region. It is also known that scattering at irregular interfaces of a short-period superlattice and impurity scattering in a double-barrier quantum well have an important influence on quantum tunnelling I–V characteristics [10, 11], and recent experiments have demonstrated that in quantum wires without impurities, the scattering from the wire boundary roughness gives rise to a large positive magneto-resistance [12]. This positive magneto-resistance is similar to that observed in metallic thin films for which a classical explanation is possible [13]. In addition, for systems where two separate disordered reservoirs are connected by a purely ballistic region, Maslov, Barnes and Kirczenow have shown that the conductance fluctuations can be suppressed by the presence of the ballistic cavity [14].

In all of the above situations the devices possess regions where impurity scattering is important, and regions where very little impurity scattering is present. From a theoretical point of view these are difficult problems because one has to deal with a spatially non-uniform system. Furthermore, many conceptual difficulties arise concerning this 'mixed' regime of quantum transport, such as the destruction of UCF by the ballistic channels, the competition of localization effects and ballistic effects, the contributions of subbands in the presence of impurity scattering, and more importantly the role played by various length scales. So far, theoretical studies of this 'mixed' transport regime have focused on the important problem of a narrow quantum wire [12] with rough boundaries [15, 16, 17, 18], and investigations of conductance fluctuations in these systems have been limited to numerical calculations. While useful intuition has been obtained, it is nevertheless difficult to draw general conclusions from purely numerical investigations since accurate values of the conductance fluctuations as a function of system parameters are difficult to obtain. The purpose of this paper is to provide a theoretical analysis of this 'mixed' regime, giving more details than in our previous letter [19] as well as some additional results.

In particular, we have extended the diagrammatic technique [2] to deal with a dirty wire where the impurities are distributed *non-uniformly* and located near the wire boundaries, leaving the centre region of the wire free of impurities, and thus ballistic. This leads to several new features of the analysis as compared with the conventional UCF theory. We note the appearance of a new set of diagrams describing the correlated scattering across the ballistic region of the sample, the new mathematical character of the diffusion operator, and the extension of the notion of the range of the energy correlation. We will describe these formal developments in detail. After making several physically and mathematically reasonable approximations, our calculations can be carried out analytically. Our main results are the non-universal conductance fluctuation amplitudes as a function of the sample length L, for arbitrary impurity layer thickness t. For a uniform distribution of the impurities we recover the known results of UCF, while for non-uniform distributions we reveal the destruction of UCF by the ballistic region. Our results provide some answers concerning the general questions discussed above, and clearly reveal the crossover behaviour of the fluctuation amplitude from the usual quasi-1D UCF situation to that of the mixed regime. Finally, we confirm our analytical predictions by a direct numerical evaluation of the Landauer–Büttiker formula [20].

The paper is organized as follows. In the next section a simple model is presented to illustrate the difference between surface roughness scattering and the bulk scattering. We obtain useful intuition concerning the correlated scattering across the ballistic centre region

of the sample. Then in section 3 we derive the expression [19] for conductance fluctuations in the mixed transport regime where impurities are distributed in a layer near the sample boundaries. In section 4 the analytical formula is evaluated and results discussed. Section 5 presents a direct numerical evaluation of the Landauer–Büttiker formula for the dirty wire, which provides a quantitative confirmation of the analytical predictions. Finally a summary is given in section 6. The tedious algebraic analyses have been grouped into four appendices.

2. Simple model with impurities only on surfaces

To develop intuition concerning a new ingredient in the theory of the 'mixed' transport regime, we first examine a very simple two-dimensional model, putting random impurities exactly on two opposite boundaries of a sample as shown in figure 1(a). There are no impurities in the bulk region of the sample. Current flow is in the plane of this figure, parallel to the boundaries. Clearly this model mimics, to some extent, the surface roughness scattering [4, 21, 22, 23]. We deduce a general theory for this system, in particular concentrating on the renormalized energy of the electrons and the imaginary part of the electron self-energy in the single-particle approximation. Then we study the three-dimensional model as shown in figure 1(b), with impurities on all four boundaries, and current flow perpendicular to the plane of the figure. The purpose of this exercise is two-fold. First, we want to find the main differences between the non-uniform impurity scattering and the uniform bulk impurity scattering: these differences lead to a change of the transport characteristics. Second, we attempt to investigate the correlated scattering from different boundaries due to the wave-like nature of the electrons across the ballistic centre region of the sample.

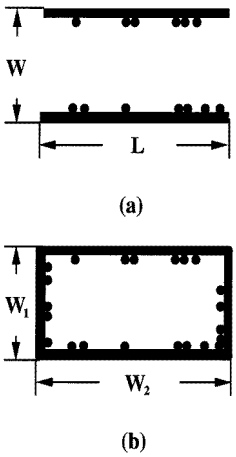

Figure 1. Schematic view of the cross sections of dirty wires. (a) For a 2D wire, impurities lie only on the upper and lower boundaries and current flows from, say, left to right. (b) A cross section for a 3D wire where impurities lie on all boundaries, and current flows, say, into the page.

We start by considering the motion of electrons in an array of scattering potentials $\mathcal{V}(\boldsymbol{x}_j - \boldsymbol{X}_i)$ located at positions $\boldsymbol{X}_i$ which are randomly placed *exactly* on the upper and lower boundaries of the wire (see figure 1(a)). The jth electron has momentum $\mathcal{P}_j$ and

effective mass m^*. Neglecting the electron–electron interaction, the Hamiltonian then reads

$$\mathcal{H} = \sum_j \frac{\mathcal{P}_j^2}{2m^*} + \sum_j \sum_i^{boundaries} \mathcal{V}(\boldsymbol{x}_j - \boldsymbol{X}_i).$$

It is convenient to approximate each potential $\mathcal{V}(\boldsymbol{x})$ as a δ-function of strength u, and then to rewrite $\mathcal{H}$ in its second-quantized form [24]. We have

$$\mathcal{H} = \sum_{\mathcal{P}} \epsilon_{\mathcal{P}} a_{\mathcal{P}}^\dagger a_{\mathcal{P}} + \sum_{\boldsymbol{q}} u[\rho_{\boldsymbol{q}}^u + \rho_{\boldsymbol{q}}^l] \sum_{\mathcal{P}} a_{\mathcal{P}+\boldsymbol{q}}^\dagger a_{\mathcal{P}} \tag{1}$$

where $a_{\mathcal{P}}^\dagger$ and $a_{\mathcal{P}}$ are creation and annihilation operators for momentum $\mathcal{P}$, $\epsilon_{\mathcal{P}}$ is the kinetic energy of the electrons, and $\rho_{\boldsymbol{q}}^u = \sum_i^{upper} \mathrm{e}^{-\mathrm{i}\boldsymbol{q}\cdot\boldsymbol{x}_i}$ and $\rho_{\boldsymbol{q}}^l = \sum_i^{lower} \mathrm{e}^{-\mathrm{i}\boldsymbol{q}\cdot\boldsymbol{x}_i}$ are the impurity densities on the upper and lower boundaries. Since impurities only lie exactly on the boundaries, namely the planes $y_i = y_1$ and $y_i = y_2$, the impurity densities can be rewritten as

$$\rho_{\boldsymbol{q}}^u = \mathrm{e}^{-\mathrm{i}q_y y_1} \sum_i^{upper} \mathrm{e}^{-\mathrm{i}\boldsymbol{q}_\parallel\cdot\boldsymbol{r}_i} \qquad \rho_{\boldsymbol{q}}^l = \mathrm{e}^{-\mathrm{i}q_y y_2} \sum_i^{lower} \mathrm{e}^{-\mathrm{i}\boldsymbol{q}_\parallel\cdot\boldsymbol{r}_i}$$

where we define $\boldsymbol{q} = \{\boldsymbol{q}_\parallel, q_y\} \equiv \{q_x, q_z, q_y\}$, $\boldsymbol{x}_i = \{\boldsymbol{r}_i, y_i\} \equiv \{x_i, z_i, y_i\}$, so that $\boldsymbol{q}_\parallel$ and r are respectively the projections of the wavevector $\boldsymbol{q}$ and space coordinate $\boldsymbol{x}_i$ on to the impurity plane.

Because the interaction between electrons is neglected, the properties defined above in terms of N-particle states of the system can be calculated in terms of a Green's function representing a single electron. The equation of motion [24] of the one-particle Green's function $\mathcal{G}(\mathcal{P}, \mathcal{P}'; t)$ is

$$\left(\mathrm{i}\frac{\partial}{\partial t} - \epsilon_{\mathcal{P}}\right)\mathcal{G}(\mathcal{P}, \mathcal{P}'; t) = \delta_{\mathcal{P}\mathcal{P}'}\delta(t) + u\sum_{\boldsymbol{q}}[\rho_{\boldsymbol{q}}^u + \rho_{\boldsymbol{q}}^l]\mathcal{G}(\mathcal{P}+\boldsymbol{q}, \mathcal{P}'; t).$$

We write the perturbation solution of the diagonal part of $\mathcal{G}(\mathcal{P}, \mathcal{P}'; t)$ in energy space, $\mathcal{G}(\mathcal{P}, \mathcal{P}; \epsilon) \equiv \mathcal{G}(\mathcal{P}; \epsilon) \equiv \mathcal{G}(\mathcal{P})$, as follows

$$\begin{aligned}\mathcal{G}(\mathcal{P}) = {} & \mathcal{G}^0(\mathcal{P}) + u\mathcal{G}^0(\mathcal{P})[\rho_{\boldsymbol{q}}^u + \rho_{\boldsymbol{q}}^l]|_{\boldsymbol{q}=0}\mathcal{G}^0(\mathcal{P}) \\ & + u^2\mathcal{G}^0(\mathcal{P})\sum_{\boldsymbol{q}}[\rho_{\boldsymbol{q}}^u + \rho_{\boldsymbol{q}}^l]\mathcal{G}^0(\mathcal{P}+\boldsymbol{q})[\rho_{-\boldsymbol{q}}^u + \rho_{-\boldsymbol{q}}^l]\mathcal{G}^0(\mathcal{P}) \\ & + u^3\mathcal{G}^0(\mathcal{P})\sum_{\boldsymbol{q}}[\rho_{\boldsymbol{q}}^u + \rho_{\mathbf{q}}^l]\mathcal{G}^0(\mathcal{P}+\boldsymbol{q}) \\ & \times \sum_{\boldsymbol{q}'}[\rho_{\boldsymbol{q}'}^u + \rho_{\boldsymbol{q}'}^l]\mathcal{G}^0(\mathcal{P}+\boldsymbol{q}+\boldsymbol{q}')[\rho_{-\boldsymbol{q}-\boldsymbol{q}'}^u + \rho_{-\boldsymbol{q}-\boldsymbol{q}'}^l]\mathcal{G}^0(\mathcal{P}) + \cdots.\end{aligned}$$

To obtain the average of the above Green's function over impurity configurations we use [24]

$$\overline{\rho_{\boldsymbol{q}_\parallel}^\alpha} = n_i\delta_{\boldsymbol{q}_\parallel,0}$$

$$\begin{aligned}\overline{\rho_{\boldsymbol{q}_\parallel}^\alpha \rho_{-\mathbf{q}_\parallel}^\beta} &= n_i^2\delta_{\boldsymbol{q}_\parallel,0} + n_i \qquad \text{if } \alpha = \beta \\ &= n_i^2\delta_{\boldsymbol{q}_\parallel,0} \qquad \text{otherwise}\end{aligned}$$

$(\alpha, \beta = l, u)$

where n_i is the number of impurities on each impurity surface, which is assumed to be the same for both surfaces. We have assumed that there is no correlation between the impurity

configurations on the upper and lower boundaries. We obtain

$$\begin{aligned}\overline{\mathcal{G}(\mathcal{P})} = {} & \mathcal{G}^0(\mathcal{P}) + u\mathcal{G}^0(\mathcal{P})\overline{[\rho^u_{\boldsymbol{q}} + \rho^l_{\boldsymbol{q}}]}|_{q=0}\mathcal{G}^0(\mathcal{P}) \\ & + u^2\mathcal{G}^0(\mathcal{P})\sum_{\mathbf{q}}\overline{[\rho^u_{\boldsymbol{q}} + \rho^l_{\boldsymbol{q}}][\rho^u_{-\boldsymbol{q}} + \rho^l_{-\boldsymbol{q}}]}\mathcal{G}^0(\mathcal{P}+\boldsymbol{q})\mathcal{G}^0(\mathcal{P}) \\ & + u^3\mathcal{G}^0(\mathcal{P})\sum_{\boldsymbol{q}}\sum_{\boldsymbol{q}'}\overline{[\rho^u_{\boldsymbol{q}} + \rho^l_{\boldsymbol{q}}][\rho^u_{\boldsymbol{q}'} + \rho^l_{\boldsymbol{q}'}][\rho^u_{-\boldsymbol{q}-\boldsymbol{q}'} + \rho^l_{-\boldsymbol{q}-\boldsymbol{q}'}]} \\ & \times\mathcal{G}^0(\mathcal{P}+\boldsymbol{q})\mathcal{G}^0(\mathcal{P}+\boldsymbol{q}+\boldsymbol{q}')\mathcal{G}^0(\mathcal{P}) + \cdots. \end{aligned} \tag{2}$$

Now we analyse the Feynman diagrams corresponding to the above Green's function equation taken to third order. As shown in figure 2, there are eleven types of irreducible impurity scattering diagram, corresponding to (2). The first diagram of figure 2 is the only first-order diagram. The second to fourth diagrams are the second-order contributions, and the others are the third-order contributions. The first-order diagram in the surface scattering problem is the same as that in the uniform bulk scattering case [24]. However from second order on, new impurity scattering diagrams appear. For example, the fourth, tenth, and eleventh diagrams in figure 2 do not exist in the uniform bulk scattering case. These diagrams correspond to the correlated scattering of electrons by impurities between different boundaries: in figure 2 we use a curved solid line to represent the electrons propagating from one surface to another surface and suffering impurity scattering at different surfaces. Note that indices α and β denote either the upper or lower surface, but $\alpha \neq \beta$.

Retaining only the second-order terms, we obtain the Green's function expression

$$\begin{aligned}\overline{\mathcal{G}(\mathcal{P})} = {} & \mathcal{G}^0(\mathcal{P}) + 2un_i[\mathcal{G}^0(\mathcal{P})]^2 + 2u^2[\mathcal{G}^0(\mathcal{P})]^2 \\ & \times\sum_{\boldsymbol{q}}\mathcal{G}^0(\mathcal{P}+\boldsymbol{q})[n_i + n_i^2(1+\cos[q_y(y_1-y_2)])\delta_{\boldsymbol{q}_\parallel,0}]\end{aligned}$$

where the term with $\cos[q_y(y_1 - y_2)]$ represents the interference and correlation of electron scattering between the upper and lower boundaries. If the impurities were distributed uniformly in the wire, then this term would lose its dependence on q_y, following an average over y_1 and y_2, but in the present case it leads to new physics in respect to conductance fluctuations. Similarly, in the following section, it leads to new results after averaging over impurities lying in layers *near* the boundaries.

From the second-order equation we read off the relevant first- and second-order irreducible self-energies

$$\begin{aligned}\Sigma^{(1)} &= 2un_i \\ \Sigma^{(2)} &= 2u^2\sum_{\boldsymbol{q}}\mathcal{G}^0(\mathcal{P}+\boldsymbol{q})[n_i + n_i^2\cos[q_y(y_1-y_2)]\delta_{\boldsymbol{q}_\parallel,0}]\end{aligned}$$

and calculate the second-order self-energy contribution using the definition of the Green's function, $\mathcal{G}^0(\mathcal{P}) = 1/(\epsilon - \epsilon_{\mathcal{P}} + \mathrm{i}0^+)$ with renormalized energy $\epsilon_{\mathcal{P}} \to \epsilon_{\mathcal{P}} + 2un_i$. We have

$$\Sigma^{(2)} = 2u^2n_i\sum_{\boldsymbol{q}}\frac{1}{\epsilon - \epsilon_{\mathcal{P}+\mathbf{q}} - 2un_i + \mathrm{i}0^+} + 2u^2n_i^2\sum_{q_y}\frac{\cos[q_y(y_1-y_2)]}{\epsilon - \epsilon_{\mathcal{P}+q_y} - 2un_i + \mathrm{i}0^+}.$$

In the above equation, the first term corresponds to the normal Born scattering [24] and gives the normal lifetime τ_n. The second term corresponds to the non-Born scattering, called anomalous scattering, and creates the anomalous lifetime τ_a. We define

$$\frac{1}{\tau_n} \equiv 4\pi u^2 n_i N_{\epsilon_F} \tag{3}$$

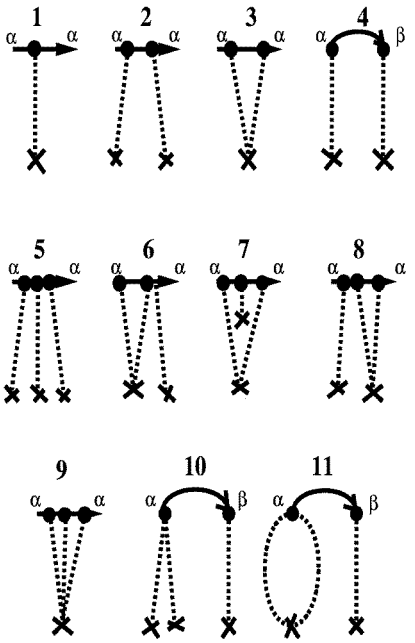

Figure 2. The impurity scattering diagrams for the case where impurities are distributed only on upper and lower boundaries. This corresponds to equation (2).

where N_{ϵ_F} is the density of states and

$$\frac{1}{\tau_a} \equiv 2u^2 n_i^2 \sum_{q_y} \cos[q_y(y_1 - y_2)]\,\delta(\epsilon - \epsilon_{\mathcal{P}+q_y} - 2un_i).$$

From the two roots of the equation $\epsilon - \epsilon_{\mathcal{P}+q_y} - 2un_i = 0$, which are

$$q_y^{(1,2)} = -\frac{\mathcal{P}_y}{\hbar} \pm \frac{1}{\hbar}\sqrt{2m\epsilon - \mathcal{P}_\parallel^2 - 4mun_i} \tag{4}$$

where a superscript (1) indicates a '+' sign and (2) a '−' sign, we rewrite the anomalous lifetime τ_a as

$$\frac{1}{\tau_a} = \frac{2mu^2 n_i^2 (y_1 - y_2)}{\hbar^2 |q_y^{(1)} - q_y^{(2)}|}[\cos[q_y^{(1)}(y_1 - y_2)] + \cos[q_y^{(2)}(y_1 - y_2)]]. \tag{5}$$

The three-dimensional version of our problem is slightly more complicated. We consider the impurities to lie on all the four boundaries, the cross section of the wire is shown in figure 1(b). We write the system Hamiltonian in the form

$$\mathcal{H} = \sum_{\mathcal{P}} \epsilon_{\mathcal{P}} a_{\mathcal{P}}^\dagger a_{\mathcal{P}} + \sum_{\boldsymbol{q}} u[\rho_{\boldsymbol{q}}^{upper} + \rho_{\boldsymbol{q}}^{lower} + \rho_{\boldsymbol{q}}^{left} + \rho_{\boldsymbol{q}}^{right}] \sum_{\mathcal{P}} a_{\mathcal{P}+\boldsymbol{q}}^\dagger a_{\mathcal{P}}$$

with two new terms $\rho_{\boldsymbol{q}}^{left}$ and $\rho_{\boldsymbol{q}}^{right}$ in the expression for the impurity density. The definitions of the two new terms are as before, but impurities lie on the left or on the right boundary. To calculate the electron irreducible self-energies up to the second order of perturbation, it is necessary to calculate the impurity configuration average. Similarly to before, since impurity configurations on different boundaries are not correlated, we obtain

$$\overline{\rho_{\boldsymbol{q}}^{upper} + \rho_{\boldsymbol{q}}^{lower} + \rho_{\boldsymbol{q}}^{left} + \rho_{\boldsymbol{q}}^{right}} = 2n_i[\delta_{\boldsymbol{q}_{\parallel xz},0} + \delta_{\boldsymbol{q}_{\parallel yz},0}]$$

and

$$\overline{[\rho_{\boldsymbol{q}}^{upper}+\rho_{\boldsymbol{q}}^{lower}+\rho_{\boldsymbol{q}}^{left}+\rho_{\boldsymbol{q}}^{right}][\rho_{-\boldsymbol{q}}^{upper}+\rho_{-\boldsymbol{q}}^{lower}+\rho_{-\boldsymbol{q}}^{left}+\rho_{-\boldsymbol{q}}^{right}]}$$
$$= 4n_i + 2n_i^2[\delta_{\boldsymbol{q}_{\parallel xz},0}+\delta_{\boldsymbol{q}_{\parallel yz},0}] + 2n_i^2[\delta_{\boldsymbol{q}_{\parallel xz},0}\cos[q_y(y_1-y_2)]$$
$$+\delta_{\boldsymbol{q}_{\parallel yz},0}\cos[q_x(x_1-x_2)]] + 8n_i^2\delta_{\boldsymbol{q},0} \tag{6}$$

where $\boldsymbol{q}_{\parallel\alpha\beta}$ $(\alpha,\beta = x, y, z)$ represents the wavevector projection onto the $\alpha\beta$-plane. We also assume, as before, that each of the four boundaries has the same impurity number n_i. We conclude that

$$\frac{1}{\tau_{(total)}^{(four)}} = 2\frac{1}{\tau_{(total)}^{(two)}}$$

where $\tau_{(total)}^{(four)}$ and $\tau_{(total)}^{(two)}$ represent the lifetimes of electrons in the four-boundary and two-boundary impurity systems, respectively. Again, $q_y^{(1)}$ and $q_y^{(2)}$ in $\tau_{(total)}^{(four)}$ are determined by the roots of equation $\epsilon - \epsilon_{\mathcal{P}+q_y} - 4un_i = 0$.

From the above analysis of this simple model we conclude that the key difference between the uniform impurity distribution problem and the non-uniform one is that in the latter case there exists an additional specific electron scattering correlation. This leads to results with some peculiar properties, which we discuss in detail in the next section.

3. Conductance fluctuations due to impurity layers

The above simple models provide intuition about what happens when the impurities are distributed at the boundaries. Namely, contributions from correlated scattering enter our analysis of the self-energies, and consequently, provide an unexpected contribution to the conductance fluctuations. However, in realistic and interesting situations, impurities do not only lie exactly on the boundaries of a wire. In general, impurities are distributed randomly in a region of finite thickness near the boundaries. Accordingly, a more realistic model would be similar to that shown in figure 3, in which impurities lie randomly along the two boundaries of the wire within impurity layers of equal thickness t.

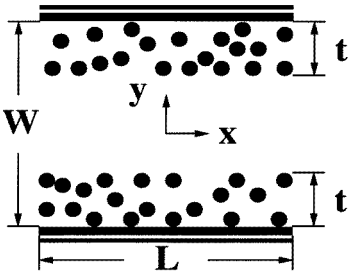

Figure 3. Schematic view of a 2D quantum wire of width W with impurity layers along the upper and lower boundaries. The impurity layer width is t.

The system Hamiltonian still retains the same form as (1). Differences first arise in the average of the impurity density and the average of the product of impurity densities in the second order of perturbation theory. For both the three-dimensional and the two-dimensional cases we have the following relations:

$$\overline{\rho_{\boldsymbol{q}}^{\alpha}} = n_i f_{q_y}(t)\delta_{\boldsymbol{q}_{\parallel},0}$$

$$\overline{[\rho_{\boldsymbol{q}}^{u}+\rho_{\boldsymbol{q}}^{l}][\rho_{\boldsymbol{q}}^{u}+\rho_{\boldsymbol{q}}^{l}]}=2n_i+2n_i[n_i|f_{q_y}(t)|^2+\mathrm{Re}[f_{q_y}(t)]]\delta_{\boldsymbol{q}_\parallel,0}$$

where ($\alpha = u, l$) and the function $f_{q_y}(t)$, which is assumed to be Gaussian, describes the impurity distribution away from the boundaries: $f_{q_y}(t)=\int_0^t \mathrm{e}^{-\gamma y^2}\mathrm{e}^{\mathrm{i}q_y y}\mathrm{d}y/\int_0^t \mathrm{e}^{-\gamma y^2}\mathrm{d}y$. The parameter γ controls the width of the distribution: a very small γ gives essentially a uniform distribution in the layer t, while a larger γ gives a diffusive distribution with higher concentration of impurities near the quantum wire boundary.

We calculate the electron lifetimes as discussed in the last section. In the three-dimensional case, we find that the normal electron lifetime is the same as (3), while the anomalous lifetime becomes

$$\frac{1}{\tau_a}=\frac{2mu^2n_iW}{\hbar^2|q_y^{(1)}-q_y^{(2)}|}\Big[n_i[|f_{q_y^{(1)}}(t)|^2+|f_{q_y^{(2)}}(t)|^2]+\mathrm{Re}[f_{q_y^{(1)}}(t)+f_{q_y^{(2)}}(t)]\Big]. \tag{7}$$

Here W is the width of the wire in the y-direction, which is actually equal to y_1-y_2 of the last section. $q_y^{(1)}$ and $q_y^{(2)}$ are still determined by the roots of the equation $\epsilon-\epsilon_{\mathcal{P}+q_y}-2un_i=0$. Since the impurity scattering strength u is small we can rewrite the expressions for $q_y^{(1)}$ and $q_y^{(2)}$ approximately, using (4)

$$q_y^{(1)}\approx 0 \tag{8}$$

and

$$q_y^{(2)}\approx -\frac{2\mathcal{P}_y}{\hbar}. \tag{9}$$

Substituting (8) and (9) into (7), we have

$$\frac{1}{\tau_a}=\frac{mu^2n_iW}{\hbar|\mathcal{P}_y|}\left[n_i[1+|f_{\mathcal{P}_y}(t)|^2]+1+\mathrm{Re}[f_{\mathcal{P}_y}(t)]\right].$$

The total electron elastic scattering lifetime is $1/\tau=1/\tau_n+1/\tau_a$. We obtain:

$$\frac{1}{\tau}=\frac{mu^2n_iLW}{\hbar^2}\left[\frac{2k_FW}{\pi}+\frac{\hbar}{|\mathcal{P}_y|L}[n_i[1+|f_{\mathcal{P}_y}(t)|^2]+1+\mathrm{Re}[f_{\mathcal{P}_y}(t)]]\right]$$

where k_F is the Fermi wavevector, and we use the three-dimensional density of one-spin states for free electrons, $N_{\epsilon_F}=\frac{2\pi V}{h^3}(2m)^{3/2}{\epsilon_F}^{1/2}$ with sample volume V. For the two-dimensional case $1/\tau$ is found to be

$$\frac{1}{\tau}=\frac{2mu^2n_iLW}{\hbar^2}\left[1+\frac{\hbar}{2|\mathcal{P}_y|L}[n_i[1+|f_{\mathcal{P}_y}(t)|^2]+1+\mathrm{Re}[f_{\mathcal{P}_y}(t)]]\right] \tag{10}$$

where $N_{\epsilon_F}=2\pi mS/h^2$ is the free-electron two-dimensional density of states for a sample of area S. The transverse momentum dependence of the electron lifetime makes the conductance fluctuation analysis much more complicated. However, an analysis is still possible after we make some physically reasonable approximations.

According to the theory of Al'tshuler, Lee and Stone [2, 3], to compute the conductance fluctuations we need to evaluate bubble–bubble diagrams as shown in figure 4. In particular the diffusion operator and the current function must be obtained. These quantities differ from those for the corresponding uniform bulk scattering case, as we will show in this section.

We first focus on the current function in the three-dimensional case. For this purpose we need to evaluate the integral of the product of four Green's functions. Because we are only interested in the limits of small momentum transfer q and frequency transfer ω, we

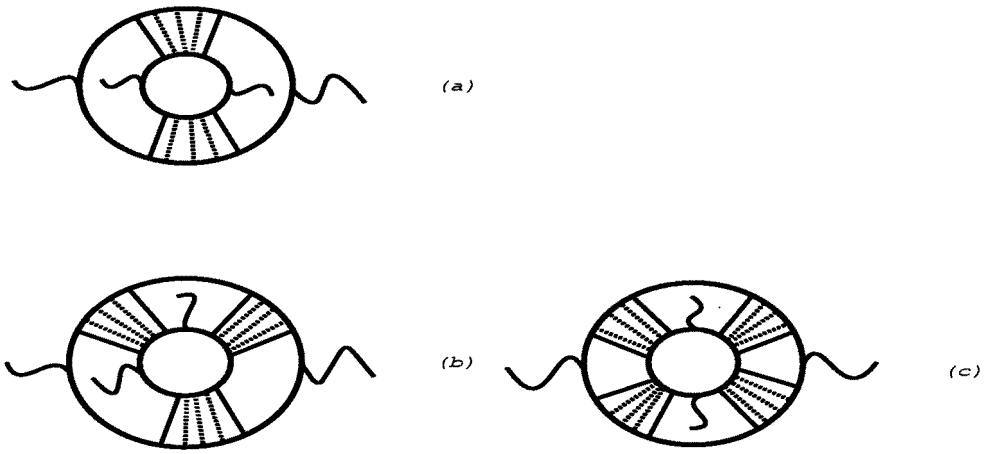

Figure 4. Conductance fluctuation diagrams including (a) double, (b) triple, and (c) quadruple bubble–bubble connections.

approximate $\tau(q_y - \mathcal{P}_y)$ by $\tau(\mathcal{P}_y)$. The tedious algebra of evaluating the product of four Green's functions is presented in Appendix A, so here we quote only the result:

$$I_1 \equiv \int \frac{\mathrm{d}\mathcal{P}}{(2\pi\hbar)^3}\mathcal{G}^R(\mathcal{P},\epsilon)\mathcal{G}^A(\mathcal{P},\epsilon-\hbar\omega)\mathcal{G}^R(\boldsymbol{q}-\mathcal{P},\epsilon)\mathcal{G}^A(\boldsymbol{q}-\mathcal{P},\epsilon-\hbar\omega)$$
$$\approx 4\pi\int \frac{\mathrm{d}\mathcal{P}_y}{(2\pi\hbar)}N_{2D}(\epsilon-\epsilon_\perp)[\tau(\mathcal{P}_y)]^3 \tag{11}$$

where $N_{2D}(\epsilon-\epsilon_\perp)$ is the two-dimensional density of states; for free electrons $N_{2D}(\epsilon-\epsilon_\perp) = N_{\epsilon_F}$. Obviously, the integral of the product of the four Green's functions, I_1, is no longer a constant as in the uniform bulk scattering case (see equation (A3) in [25]). It now depends strongly on the transverse momentum transfer $\mathcal{P}_y$. This leads to anisotropic characteristics in momentum space.

The diffusion operator for the three-dimensional case also differs from its counterpart for uniform scattering which is proportional to $Dq^2 - \mathrm{i}\omega$, where D is the diffusion constant. For the case of non-uniform scattering we give a detailed derivation of this operator in Appendix B, and obtain the real space expression

$$\frac{1}{u^2 n_i} - \frac{3}{4}\Gamma^{(1)} - \mathrm{i}\omega\Gamma^{(2)} - \frac{1}{3}v_F^2\Gamma^{(3)}\nabla^2 + \mathrm{i}v_F\Gamma^{(4)}\frac{\partial}{\partial y}\left(\frac{\partial}{\partial x}+\frac{\partial}{\partial y}+\frac{\partial}{\partial z}\right) - \frac{1}{4}\Gamma^{(5)}\frac{\partial^2}{\partial y^2}. \tag{12}$$

This expression for the diffusion operator in three-dimensional real space determines the electron scattering characteristics. Once the eigen-solutions of this operator are found, we are able in principle to calculate the electron scattering vertex functions, and using the same techniques as described in [25] to compute the conductance fluctuations. In practice, because the eigenfunctions of the diffusion operator are no longer an orthogonal set, it does not seem possible to solve the eigenvalue problem (12) in an exactly analytical fashion. Thus further approximations are needed to advance our analysis.

Of course, the same difficulties exist for the simpler two-dimensional problem. Thus, without loss of generality, we will proceed by investigating the conductance fluctuations of a two-dimensional quantum wire, where our results can be checked by extensive numerical simulations. Clearly a similar procedure could be applied in three dimensions. From the

detailed algebra of Appendix C, we thus obtain the eigenvalue equation for the diffusion operator in two dimensions:

$$\left[\boldsymbol{C}_0 + \boldsymbol{C}_1\frac{\partial^2}{\partial x^2} + \boldsymbol{C}_2\frac{\partial^2}{\partial y^2} + \boldsymbol{C}_3\frac{\partial^2}{\partial x\partial y}\right]\boldsymbol{Q}_m(\boldsymbol{x}) = \lambda_m\boldsymbol{Q}_m(\boldsymbol{x}) \tag{13}$$

where the $\boldsymbol{C}_i$ are constants defined in Appendix C.

Although the eigenfunctions of this operator are not an orthogonal set, fortunately, however, we can show through explicit numerical solution (see Appendix D), that the eigenvalues λ_m fall into many densely packed clusters: the eigenvalues in each cluster are very close to each other. Numerically we can evaluate the overlap integrals of any two normalized eigenfunctions corresponding to different eigenvalues. The results turn out to be either near 1 for those eigenfunctions belonging to the same cluster, or near 0 for eigenfunctions from different clusters. This is not surprising in practice since we can easily check that $|\boldsymbol{C}_3| \ll |\boldsymbol{C}_1|$ or $|\boldsymbol{C}_2|$. Thus it is a reasonable approximation to regard the eigenfunctions as being orthogonal, which allows us to use the same equation (equation (A7) in [25]) to calculate the diffusive vertex function.

Using the current function determined by the integral I_1 of (11) and the diffusion propagator as properly expanded using the eigenfunctions of the diffusion operator, we can write in general the three exact conductance fluctuation expressions, $\boldsymbol{F}_a$, $\boldsymbol{F}_b$, and $\boldsymbol{F}_c$ which are related to the three types of bubble–bubble connection Feynman diagram in figure 4. For the details we refer interested readers to [25]. The final results are:

$$\boldsymbol{F}_a = N_a\left[\frac{v_F^2 n_i u^2\Gamma^{(3)}}{L^2}\right]^2\sum_m\sum_{m'}\frac{[\int \mathrm{d}\boldsymbol{x}\,\boldsymbol{Q}_m^*(\boldsymbol{x})\boldsymbol{Q}_{m'}(\boldsymbol{x})][\int \mathrm{d}\boldsymbol{x}\,\boldsymbol{Q}_{m'}^*(\boldsymbol{x})\boldsymbol{Q}_m(\boldsymbol{x})]}{\lambda_m\lambda_{m'}} \tag{14}$$

$$\boldsymbol{F}_b = -N_b L^2\left[\frac{v_F^2 n_i u^2\Gamma^{(3)}}{L^2}\right]^3\sum_m\sum_{m'}\sum_{m''}\frac{[\int \mathrm{d}\boldsymbol{x}\,\boldsymbol{Q}_m(\boldsymbol{x})\boldsymbol{Q}_{m'}^*(\boldsymbol{x})]}{\lambda_m}\times\frac{[\int \mathrm{d}\boldsymbol{x}\,\boldsymbol{Q}_{m'}(\boldsymbol{x})\frac{\partial}{\partial y}\boldsymbol{Q}_{m''}^*(\boldsymbol{x})][\int \mathrm{d}\boldsymbol{x}\,\boldsymbol{Q}_{m''}(\boldsymbol{x})\frac{\partial}{\partial y}\boldsymbol{Q}_m^*(\boldsymbol{x})]}{\lambda_{m'}\lambda_{m''}} \tag{15}$$

$$\boldsymbol{F}_c = N_c L^4\left[\frac{v_F^2 n_i u^2\Gamma^{(3)}}{L^2}\right]^4\sum_m\sum_{m'}\sum_{m''}\sum_{m'''}\frac{[\int \mathrm{d}\boldsymbol{x}\,\boldsymbol{Q}_m(\boldsymbol{x})\frac{\partial}{\partial y}\mathbf{Q}_{m'}^*(\boldsymbol{x})][\int \mathrm{d}\boldsymbol{x}\,\boldsymbol{Q}_{m'}(\mathbf{x})\frac{\partial}{\partial y}\boldsymbol{Q}_{m''}^*(\boldsymbol{x})]}{\lambda_m\lambda_{m'}}\times\frac{[\int \mathrm{d}\boldsymbol{x}\,\boldsymbol{Q}_{m''}(\boldsymbol{x})\frac{\partial}{\partial y}\mathbf{Q}_{m'''}^*(\boldsymbol{x})][\int \mathrm{d}\boldsymbol{x}\,\boldsymbol{Q}_{m'''}(\mathbf{x})\frac{\partial}{\partial y}\boldsymbol{Q}_m^*(\boldsymbol{x})]}{\lambda_{m''}\lambda_{m'''}}. \tag{16}$$

Using the above formula we can obtain the full expression of the conductance fluctuations in the absence of a magnetic field. Similarly to [25], we finally find the amplitude of the conductance fluctuations:

$$\boldsymbol{F}^{total} = 2(\boldsymbol{F}_a + \boldsymbol{F}_b + \boldsymbol{F}_c). \tag{17}$$

4. Discussion of the analytical results

In the last section we derived the expression for the conductance fluctuations, equations (14)–(17), for our non-uniform system. However, due to the complicated appearance of the result, it remains difficult to gain insight into the situation. As discussed previously, a significant complication is due to the transverse momentum dependence of the electron lifetime. If in a gross approximation this is neglected, the theory is dramatically simplified, and gives us a rough estimate of the conductance fluctuations together with the needed intuition. We first investigate this limit before presenting the results of the full analysis.

Neglecting the momentum transfer q_y dependence on τ, we obtain, instead of (26) of Appendix B, the 2D integral

$$I_2 = \frac{1}{\hbar}\int \mathrm{d}\mathcal{P}_y N_{1D}(\epsilon - \epsilon_\perp)\left[\tau(\mathcal{P}_y)(1 + \mathrm{i}\omega\tau(\mathcal{P}_y) - \mathrm{i}v_F q\tau(\mathcal{P}_y) - v_F^2 q^2[\tau(\mathcal{P}_y)]^2)\right].$$

Using the definitions of $\Gamma^{(1)}$, $\Gamma^{(2)}$, and $\Gamma^{(3)}$ defined in (30) of Appendix C, we have

$$I_2 = \Gamma^{(1)} + \mathrm{i}\omega\Gamma^{(2)} - \mathrm{i}q v_F\Gamma^{(2)} - \frac{1}{2}v_F^2 q^2\Gamma^{(3)}. \tag{18}$$

We further approximate the momentum $\mathcal{P}_y$ in the electron lifetime $\tau(\mathcal{P}_y)$ by its average value $\overline{\mathcal{P}_y}$, so that the diffusion operator becomes

$$\frac{1}{u^2 n_i}\left[1 - \frac{2\pi u^2 n_i N_{2D}(\epsilon)\tau}{\hbar}\left[1 + \mathrm{i}\omega\tau - \mathrm{i}v_F q\tau - \frac{1}{2}v_F^2 q^2\tau^2\right]\right]. \tag{19}$$

We emphasize that the scattering time τ which appears above is not given by the corresponding expression for the uniform bulk scattering, namely $\hbar/\tau \neq 2\pi u^2 n_i N_{2D}(\epsilon)$. It is given by the expression in (10), with $\mathcal{P}_y$ replaced by its average value. We can thus rearrange (19) as

$$\frac{1}{u^2 n_i}\left[1 - \frac{2\pi u^2 n_i N_{2D}(\epsilon)\tau}{\hbar}\left[\frac{1}{2} + \mathrm{i}\omega\tau - \frac{1}{2}v_F^2\tau^2\left(q + \frac{\mathrm{i}}{v_F\tau}\right)^2\right]\right].$$

Further, and for the same reason discussed in Appendix B, we find that $|\mathrm{i}/v_F\tau| \ll q$, so that the diffusion operator takes the standard form with a term proportional to q^2:

$$\frac{1}{u^2 n_i}\left[1 - \frac{2\pi u^2 n_i N_{2D}(\epsilon)\tau}{\hbar}\left[\frac{1}{2} + \mathrm{i}\omega\tau - \frac{1}{2}v_F^2\tau^2 q^2\right]\right]. \tag{20}$$

The eigenfunctions of this operator are precisely the same as those for the case of uniform bulk scattering, as described in [25], if we consider the same boundary conditions, but the eigenvalues are different.

At this point, we verify that in the appropriate limit our theory recovers the results for uniform bulk scattering as described in [25]. When the impurities in the wire are distributed completely uniformly, the electron lifetime τ becomes a constant, and in all the above calculations for our two-dimensional system we replace

$$\int \mathrm{d}\mathcal{P}_y N_{1D}(\epsilon - \epsilon_\perp)\int \mathrm{d}\epsilon' \to 2\pi N_{2D}(\epsilon)\int \frac{\mathrm{d}\Omega_{\boldsymbol{k}}}{S_z}\int \mathrm{d}\epsilon'.$$

We also note that the third term on the right-hand side of (18) vanishes since

$$\int \frac{\mathrm{d}\Omega_{\boldsymbol{k}}}{S_z} v_F(\boldsymbol{k})[\cdots] = 0.$$

In addition we have

$$\int \frac{\mathrm{d}\Omega_{\boldsymbol{k}}}{S_z}[v_F(\boldsymbol{k})]^2 = \frac{1}{2}v_F^2.$$

Therefore (18) becomes

$$I_2 = \frac{2\pi}{\hbar}N_{2D}(\epsilon)\tau\left[1 + \mathrm{i}\omega\tau - \frac{1}{2}v_F^2 q^2\tau^2\right]$$

and the diffusion operator is

$$\frac{1}{u^2 n_i}\left\{1 - 2\pi u^2 n_i\left[\frac{1}{\hbar}N_{2D}(\epsilon)\tau\left[1 + \mathrm{i}\omega\tau - \frac{1}{2}v_F^2 q^2\tau^2\right]\right]\right\}.$$

Using $\overline{h}/\tau = 2\pi u^2 n_i N_{2D}(\epsilon)$, the diffusion operator reduces exactly to the same form as for the uniform case [25, 26],

$$\frac{1}{u^2 n_i}\left[\mathrm{i}\omega\tau - \frac{1}{2}v_F^2 q^2 \tau^2\right] = \frac{\tau}{u^2 n_i}[\mathrm{i}\omega - Dq^2]$$

with $D = \frac{1}{2}v_F^2\tau$.

Finally, to obtain numerical values of the conductance fluctuations for the two-dimensional dirty wire, we need to evaluate the final expressions (14)–(16) numerically. This involves a numerical determination of the eigenfunctions and eigenvalues of the diffusion operator, using the prescription discussed in the last section. A very important point with deep physical meaning is the determination of the so-called electron energy correlation range [25, 27] $\triangle E_c$. This quantity is essentially the energy transfer in the two-particle scattering vertices, namely the energy transfer between the two diffusion bubbles. In our numerical calculations we replace the energy transfer ω by this quantity [25]. Physically $\triangle E_c$ gives an energy scale: for a temperature $k_B T \gg \triangle E_c$ the phases of the various transmission paths differ significantly so that the contributions of these paths average out in our fluctuation calculations. In other words, a change in the applied voltage by $\triangle E_c/e$ with a carrier charge e would alter the electron energy by $\triangle E_c$, and this is sufficient to cause phase shifts to individual paths such that they become uncorrelated with their initial values. As a consequence of impurity scattering, the phase differences between each pair of paths will change in an essentially random manner, so that these paths will not contribute to the conductance fluctuations [28].

The discussion of $\triangle E_c$ can be traced back to the work of Thouless who formulated a scaling theory description of the electron localization problem [29] which was important for subsequent developments. It was concluded that (at least in one dimension) the conductance g is proportional to $(\triangle E/\triangle W)^2$[30], where $\triangle E$ and $\triangle W$ are respectively the bandwidth of the electron eigenstates and the energy level spacing in a D-dimensional sample with volume L^D. The energy correlation range is related to the energy spread of a wavepacket, and thus to $\triangle W$ (where $g \sim O(1)$), a quantity that can easily be estimated for both the ballistic and the diffusive transport regimes.

In the ballistic case, the energy correlation range is therefore given by $\triangle k L \sim 1$ or

$$\triangle E_c \sim \frac{\overline{h} v_F}{L} \qquad \text{for} \quad L \ll l. \tag{21}$$

Following Imry [27], we rewrite this expression as $\overline{h} v_F/\sqrt{LW}$. In the diffusive regime the distance travelled by an electron across the system is given by $v_F L^2/D$. Replacing L in (21) by this length, we find

$$\triangle E_c \sim \frac{\overline{h} D}{L^2} \qquad \text{for} \quad L \gg l. \tag{22}$$

This energy has been shown [31] to be identical to the parameter $\triangle W$, consistent with our expectations.

In our non-uniform system, there exist two separated regions. One has an impurity distribution in the layers of thickness t along the boundaries; this is the diffusive region. The other is the impurity-free central region which permits ballistic transport. Thus the correlation energy $\triangle E_c$ should be an admixture of both diffusive and ballistic contributions. Considering the probabilities of electrons being in each region, and using the above results, the simplest form for $\triangle E_c$ is

$$\triangle E_c \sim \frac{2t}{W}\frac{v_F^2 \overline{\tau(\mathcal{P}_y)}\overline{h}}{dL^2} + \left(1 - \frac{2t}{W}\right)\frac{\overline{h} v_F}{\sqrt{LW}}. \tag{23}$$

Here $\overline{\tau(\mathcal{P}_y)}$ is the average value of $\tau(\mathcal{P}_y)$ over momentum $\mathcal{P}_y$; $d = 2$ or 3 for 2D or 3D wires; and the factors $2t/W$ and $(1 - 2t/W)$ refer to the probability of the electron being located in the impurity region and the central ballistic region, respectively. Using this choice of $\triangle E_c$ to replace the energy transfer ω in the diagrammatic calculations, we can obtain the final numerical results.

A first hint of the effects of the non-uniform impurity distribution can be obtained by using the approximate formula (19), valid when the $\mathcal{P}_y$ dependence of the electron relaxation time is averaged out. As discussed above, this gross approximation makes the algebra very similar to that for the usual UCF calculations [25] since the diffusion propagator becomes isotropic as shown in (20). The numerical curves of conductance fluctuations $[rms(g)]^2$ as a function of the wire length L for various impurity layer thicknesses t were shown in figure 1 of [19] for several given t. We refer interested readers to [19] for numerical details. Here we merely mention that the conventional UCF is obtained for $t = W/2$, while for smaller t the conductance fluctuations decay smoothly to zero as the length of the wire is increased. Such a decay is also faster for smaller t. These observations can be understood as resulting from the effect of localization [15, 16, 32] for which a discussion is provided in [19].

When we include all the anisotropies, the general behaviour of the conductance fluctuations as a function of the wire length L is similar to the approximate results discussed above; the numerical curves were shown in figure 2 of [19]. Essentially, the conductance fluctuation $[rms(g)]^2$ still drops rapidly as L increases and becomes very small for large values of L, and there are clear oscillations of $[rms(g)]^2$ as L is increased [19]. The oscillations are not present in the 'isotropic theory', since it does not respect the lateral anisotropy. We have also checked that when $[rms(g)]^2$ is plotted against other parameters such as the Fermi energy or the impurity layer thickness t, similar oscillations are observed, as shown in figure 5. This indicates that the oscillations result from resonance behaviour since wavefunctions and their derivatives must match across the different layers in the wire. Finally, our numerical values obtained by evaluating (17) are consistent [19] with those obtained from simulations of rough boundary scattering [18] if we interprete the thickness t as playing the role of the roughness amplitude.

5. Numerical simulations

An alternative approach to the problem studied so far is provided by direct numerical simulations, employing the Landauer–Büttiker formula

$$G = \frac{2e^2}{h} \sum_{i=1}^{N} T_i \tag{24}$$

to compute the conductance and its fluctuations. Here $\{T_i\}$ is the transmission coefficient of mode i, so that we must compute the transmission coefficients for all the subbands above the propagating threshold for a given Fermi energy. This not only provides a quantitative check of our analytical results, but also shows how the contributions of successive propagating subbands contribute to the conductance fluctuations.

For the simulation we use a hard wall impurity potential to simulate the δ-function interaction between electrons and impurities which was used in our analysis. We imagine that the dirty quantum wire of figure 3 is attached to perfect leads with the same width and hard wall potential. Then the dirty wire region provides the scattering. Electrons come from the left-hand lead, scatter in the dirty wire region, and reflect back or transmit through to

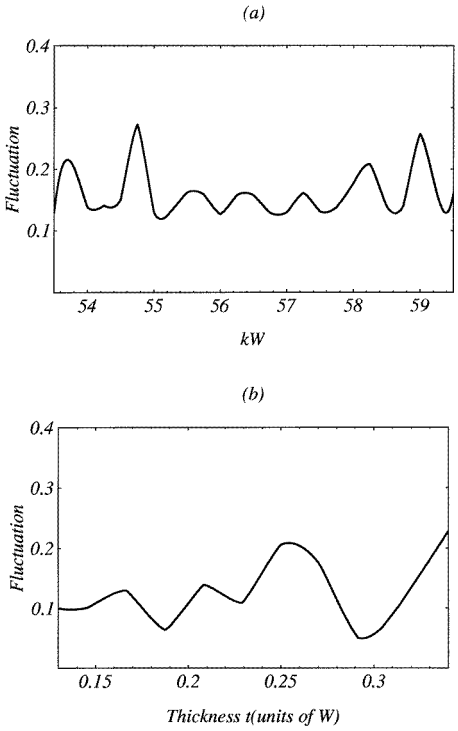

Figure 5. The conductance fluctuation oscillations (in units of $(e^2/h)^2$) as a function of (a) the Fermi energy, with $t = W/6$; and (b) the impurity layer thickness t, with $kW = 55$.

the right-hand lead. The quantum scattering of electrons is solved by using a finite element numerical scheme [33, 34] for the single-electron effective mass Schrödinger equation.

Essentially, we discretize the scattering region into a fine grid of triangles. The wavefunctions are numerically evaluated inside this region, and then matched at its boundaries to the wave functions inside the leads, which are evaluated separately. This matching procedure gives the various transmission coefficients. The finite element method reduces the complicated scattering problem into a sparse matrix calculation and is very generally applicable to quantum device simulations: it allows us to obtain quantitatively accurate results. Typically we used 550 to 1400 (the largest was 5000) independent impurity configurations for the ensemble averaging of each subband.

In figure 6(a) and (b) we show the conductance as a function of sample number for two wires with $t = W/2$ (uniform case) and $t = W/6$ (non-uniform case), within the first propagation subband. It is evident that in the uniform case the conductance is smaller because of more impurity scattering. For the 4000 impurity configurations examined, the first subband transmission gives an average conductance value around $g \sim 0.25$ with quite large sample-to-sample fluctuations. In the non-uniform case of $t = W/6$ the conductance is larger because there are fewer impurities due to the presence of the ballistic region. For this case we find that averaging over only 1400 impurity configurations provides statistically significant values for the various physical quantities.

To calculate the *sample-to-sample* conductance fluctuations for our quantum wires we need to fix the energy of the incoming electrons. In particular, the energy must not be so low that conduction is inhibited [32]. To determine a reasonable energy, we recall what is

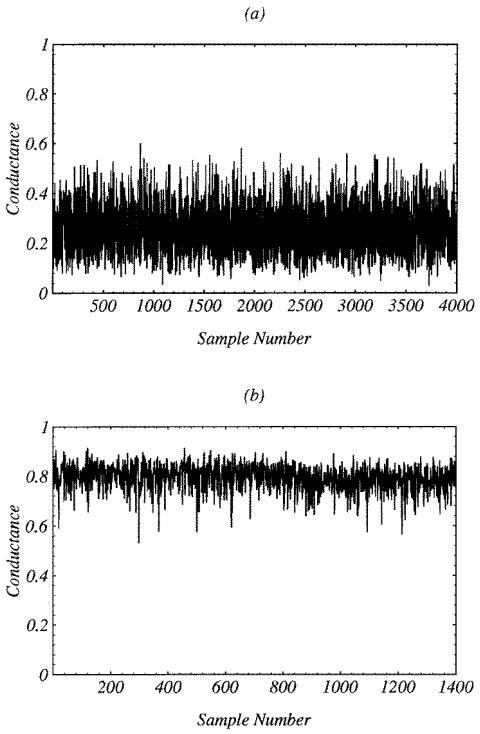

Figure 6. Conductance of different impurity configurations (in units of e^2/h) in the first subband: (a) uniform case ($t = W/2$) with $n_i = 40$, and (b) non-uniform case ($t = W/6$) with $n_i = 26$. For both wires $L = W$.

usually done in the UCF literature. In [25], Lee, Stone and Fukuyama gave a comparison of sample-to-sample conductance fluctuations to those due to changing the applied magnetic field or the Fermi energy in a single sample. Using the Anderson model with disorder, their numerically simulated data were found qualitatively to support the 'ergodic hypothesis'. Accordingly, we first used a single sample and computed its conductance fluctuations by varying the energy. We then averaged the results over energy ranges around $10 \times \triangle E_c$. For a wire with a uniform impurity distribution, i.e. $t = W/2$, and for the first subband, our results are shown in figure 7. Figures 7(a), (b) were obtained for energy averaging over $8 \times \triangle E_c$; figures 7(c), (d) are for $10 \times \triangle E_c$; and figures 7(e), (f) are for $15 \times \triangle E_c$. From these results it is clear that both the conductance and its fluctuations have strong energy dependences at low energy, and weak dependence at high energy. In other words, the UCF regime is found at higher energies [32]. In particular, our data show that at around $kW = 55$ (energy $E = 16.2$ meV), the conductance fluctuations are almost independent of the Fermi energy. Thus, in all our subsequent calculations of the sample-to-sample fluctuations we fix the incoming electron energy at this value.

Another interesting finding of our simulations is that the correlation energy in general becomes larger as we decrease the thickness of the impurity layers. This is shown in figure 8, because the peak-to-peak distance [25, 27] in energy units is essentially $\triangle E_c$. Such behaviour is reasonable since with the decrease of the impurity layer thickness, the ballistic region becomes more dominant, so enhancing the correlation range. In the limit of no impurities, we have a perfect straight quantum wire and no conductance fluctuations. In

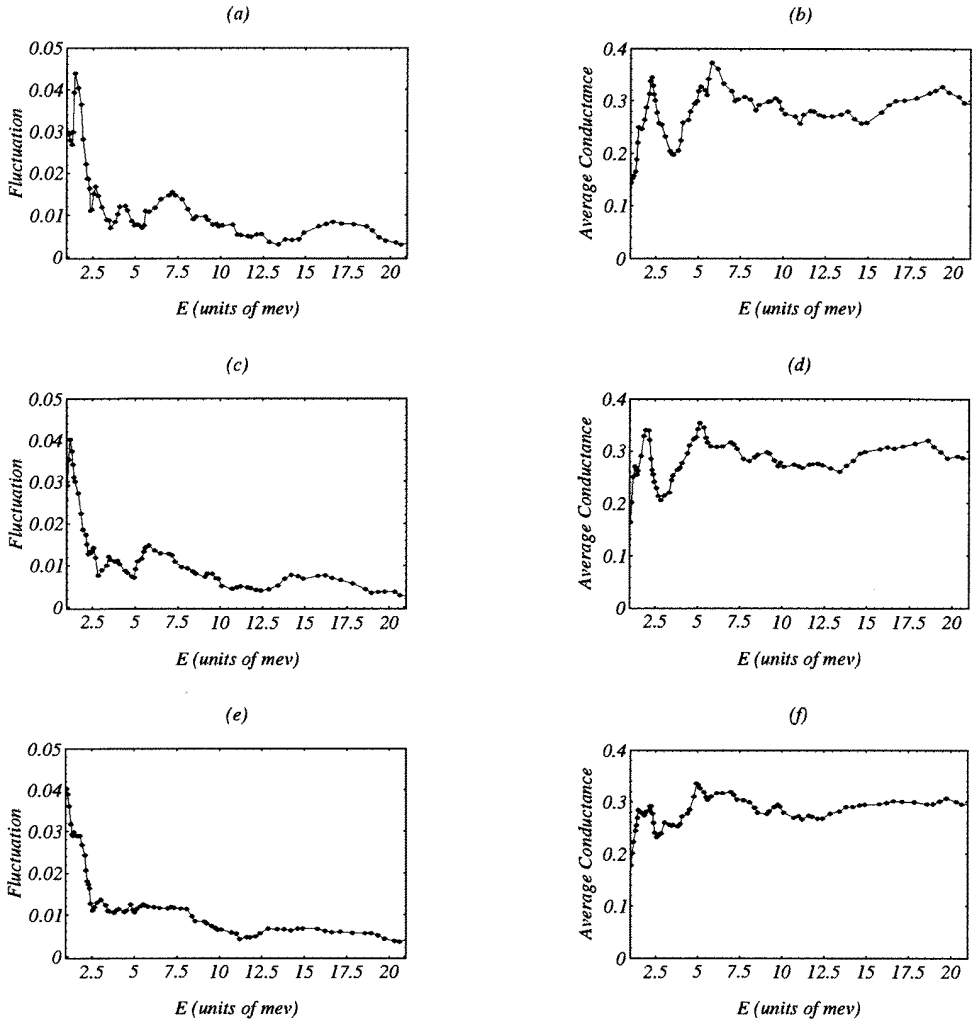

Figure 7. The conductance fluctuation amplitude (in units of $(e^2/h)^2$) and conductance (in units of e^2/h) averaged over different multiples of the correlation energy $\triangle E_c$: (a) and (b) $8 \times \triangle E_c$; (c) and (d) $10 \times \triangle E_c$; (e) and (f) $15 \times \triangle E_c$.

this case $\triangle E_c \to \infty$.

For the incoming electron energy $kW = 55$ there are 17 transport subbands to be computed individually, each requiring to be averaged over a large ensemble of samples as discussed above. The contributions of these 17 subbands to the conductance and to the conductance fluctuations for $t = W/6$ are shown in figure 3 of [19] for wire length $L = W$, and here in figure 9 for $L = 2W$. From these figures it is clear that the impurity-averaged conductance of each successively higher subband is progressively smaller. This is because the higher the subband, the smaller its longitudinal (x-direction) momentum, and with smaller longitudinal momentum it is more difficult for an electron to traverse the dirty wire. This is also consistent with the numerical simulations of rough boundary scattering [15, 16]. For both values of L, the conductance shows almost identical behaviour as a function of

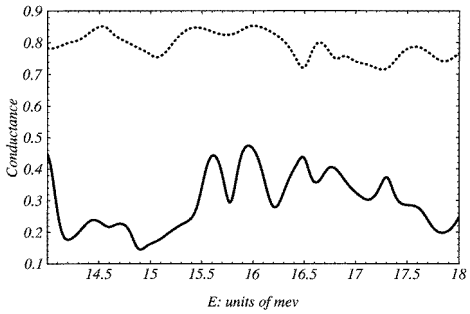

Figure 8. Conductance (in units of e^2/h) as a function of the Fermi energy. The solid line is for the uniform case ($t = W/2$) and the dashed line is for the non-uniform case ($t = W/6$).

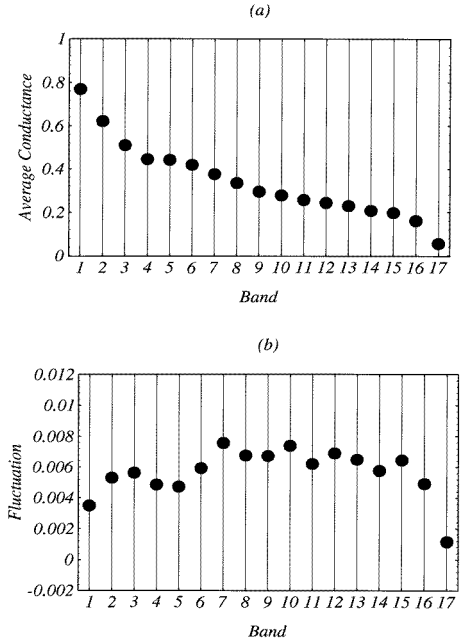

Figure 9. Results from the finite element numerical simulation for $L = 2W$. (a) The impurity averaged conductance (in units of e^2/h) for each of the 17 subbands. (b) The impurity averaged fluctuations $[rms(g)]^2$ (in units of $(e^2/h)^2$) for all the subbands. The system parameters are the same as those in the theoretical analysis.

subband. This is understandable since the conductance itself is determined largely by the ballistic region and the ballistic transport is independent of the wire length [1]. On the other hand, the conductance fluctuations do show differences for the two lengths: they are largely determined by the impurity layers so that the wire length plays a role. In addition as seen in figure 3 of [19] and figure 9 here, the first and last subbands contribute less to the fluctuations than the others. This is due to the upper and lower bounds of the conductance which each transport subband can contribute: e^2/h or zero. Since the lowest and highest subbands contribute values close to these bounds (see figure 3 of [19] and figure 9; see also figure 5), their fluctuations are limited. Finally we also notice that the contributions of the

individual subbands to the fluctuations seem to be more uniform in the longer wire. We believe that this is because longer wires provide more impurity scattering which leads to similar interference events for all subbands.

When adding up all the contributions according to the Landauer–Büttiker formula we obtain the conductance fluctuations for the two wires: for $L = W$[19] we obtained $0.13 \pm 0.01\ (e^2/h)^2$; for $L = 2W$ it is $0.09 \pm 0.01\ (e^2/h)^2$. The error bars came from the impurity averaging. For these same wires our analytical theory predicted $0.129\ (e^2/h)^2$ and $0.082\ (e^2/h)^2$, so that our simulation results are in reasonable agreement with our analytical predictions.

6. Summary

The theory of conductance fluctuations in the mesoscopic regime has been very successful in describing the anomalies of quantum transport at low temperatures. It predicts a universal conductance fluctuation at zero temperature. The reason is that in the mesoscopic regime the phase coherence length is the largest length scale: this implies that the situation is controlled by the relative phase information of the various quantum paths in a sample dominated by diffusive scattering.

This theory for the mesoscopic regime has only been applied to systems where the impurities are uniformly distributed. However, in this paper we show that it can be generalized to cases where the impurity distribution is not uniform. In particular we analytically investigate the 'mixed' transport regime where both mesoscopic and ballistic characteristics play a role. We believe this is a useful formal theoretical step: the non-uniform dirty wire leads to a new set of Feynman diagrams describing the correlated impurity scattering across the wire; it requires a careful examination of the anisotropic diffusion operator and its mathematical character; and the physical concept of the energy correlation range must be generalized. With these modifications we are able to predict the nature of conductance fluctuations in a 'dirty wire' system, and in particular we find that while the conductance is largely controlled by the ballistic region, its fluctuations are essentially controlled by the impurity layers. Because of the presence of a ballistic region, the conductance fluctuations are not universal and depend on system parameters such as the impurity layer thickness t. The fluctuations decay with the wire length L for a given t, and such a decay is faster for wires with smaller t due to electron localization effects in the impurity layers. The general behaviour predicted by our analytical approach is consistent with previous numerical simulations of roughness scattering, and is quantitatively consistent with our numerical simulations for two wires. From the device application point of view, it is important to have a detailed understanding of the sample-dependent non-universal transport characteristics of various quantum conductors, and the diagrammatic formulation presented here provides a first analytical step in this direction.

In this paper we have used two different theoretical approaches, the Feynman diagrammatic technique and the finite element numerical simulation method, to study the conductance fluctuations of electron transport in the 'mixed' regime. The work presented here includes a number of technical advances and developments which are useful for the studies of other quantum transport phenomena in semiconductor nanostructures. For instance, we can extend the diagrammatic theory used here to study the same dirty wire (non-uniform impurity distribution) but including an applied magnetic field. Secondly, the diagrammatic analysis can be extended to include a non-zero temperature. These are difficult problems, whose solution will definitely improve our understanding of the important 'mixed' transport regime. Concerning numerical simulations, we have used a finite element

scattering approach with no fitting parameters to check our analytical predictions. Although only two systems were simulated because of the requirement of exceedingly large computer resources†, our theoretical picture is quantitatively confirmed. Simplified calculations, based perhaps on tight binding models, may overcome these limitations and provide further results for the 'mixed' transport regime. We hope to report such investigations in the future.

Acknowledgements

We thank Dr C C Wan for useful discussions on the mathematical treatment of the diffusive operator. We gratefully acknowledge support by the Natural Sciences and Engineering Research Council of Canada and le Fonds pour la Formation de Chercheurs et l'Aide à la Recherche de la Province du Québec.

Appendix A. The 3D calculation of I_1

The calculation of the current function in three dimensions (3D), or two dimensions, requires the integral of the product of four Green's functions [25]. In the limits of small momentum and frequency transfers, $\tau(q_y - \mathcal{P}_y) \approx \tau(\mathcal{P}_y)$. Thus this integral becomes

$$\begin{aligned}
I_1 \equiv \int \frac{\mathrm{d}\mathcal{P}}{(2\pi\hbar)^3}\mathcal{G}^R(\mathcal{P},\epsilon)\mathcal{G}^A(\mathcal{P},\epsilon-\hbar\omega)\mathcal{G}^R(\boldsymbol{q}-\mathcal{P},\epsilon)\mathcal{G}^A(\boldsymbol{q}-\mathcal{P},\epsilon-\hbar\omega)\\
&= \int \frac{\mathrm{d}\mathcal{P}_y}{(2\pi\hbar)}\int \frac{\mathrm{d}\mathcal{P}_\parallel}{(2\pi\hbar)^2}\frac{1}{\epsilon-\epsilon_\mathcal{P}-\mathrm{i}\frac{\hbar}{2\tau(\mathcal{P}_y)}}\,\frac{1}{\epsilon-\epsilon_\mathcal{P}+\hbar\omega+\mathrm{i}\frac{\hbar}{2\tau(\mathcal{P}_y)}}\\
&\quad\times\frac{1}{(\epsilon-\hbar v_F q)-\epsilon_\mathcal{P}-\mathrm{i}\frac{\hbar}{2\tau(\mathcal{P}_y)}}\,\frac{1}{(\epsilon-\hbar v_F q)-\epsilon_\mathcal{P}+\hbar\omega+\mathrm{i}\frac{\hbar}{2\tau(\mathcal{P}_y)}}\\
&= \int \frac{\mathrm{d}\mathcal{P}_y}{(2\pi\hbar)}\int N_{2D}(\epsilon-\epsilon_\perp)\mathrm{d}\epsilon_\parallel\\
&\quad\times\frac{1}{\epsilon_\parallel+\epsilon_\perp-\epsilon_\mathcal{P}-\mathrm{i}\frac{\hbar}{2\tau(\mathcal{P}_y)}}\,\frac{1}{\epsilon_\parallel+\epsilon_\perp-\epsilon_\mathcal{P}+\hbar\omega+\mathrm{i}\frac{\hbar}{2\tau(\mathcal{P}_y)}}\\
&\quad\times\frac{1}{(\epsilon_\parallel+\epsilon_\perp-\hbar v_F q)-\epsilon_\mathcal{P}-\mathrm{i}\frac{\hbar}{2\tau(\mathcal{P}_y)}}\,\frac{1}{(\epsilon_\parallel+\epsilon_\perp-\hbar v_F q)-\epsilon_\mathcal{P}+\hbar\omega+\mathrm{i}\frac{\hbar}{2\tau(\mathcal{P}_y)}}\\
&= 2\pi\mathrm{i}\int \frac{\mathrm{d}\mathcal{P}_y}{(2\pi\hbar)}N_{2D}(\epsilon-\epsilon_\perp)\frac{1}{\hbar\omega+\mathrm{i}\frac{\hbar}{\tau(\mathcal{P}_y)}}\,\frac{(-2)}{(\hbar\omega+\mathrm{i}\frac{\hbar}{\tau(\mathcal{P}_y)})^2-(\hbar v_F q)^2}\\
&\approx 4\pi\int \frac{\mathrm{d}\mathcal{P}_y}{(2\pi\hbar)}N_{2D}(\epsilon-\epsilon_\perp)\left[\frac{\tau(\mathcal{P}_y)}{\hbar}\right]^3\frac{1}{(1-\mathrm{i}\omega\tau(\mathcal{P}_y))^3}\\
&\approx 4\pi\int \frac{\mathrm{d}\mathcal{P}_y}{(2\pi\hbar)}N_{2D}(\epsilon-\epsilon_\perp)[\tau(\mathcal{P}_y)]^3 \qquad (25)
\end{aligned}$$

with $\epsilon_\parallel \equiv \mathcal{P}_\parallel^2/2m$, $\epsilon_\perp \equiv \mathcal{P}_y^2/2m$, representing the single-electron energies along the two-dimensional xz-plane and the y-direction. $N_{2D}(\epsilon-\epsilon_\perp)$ is the two-dimensional density of states, and the expression for the single-electron Green's function in momentum

† For one set of system parameters (t, L) and averaging over 1000 impurity configurations for each of the 17 propagating subbands, the total computation took about 1100 CPU hours on a SGI R8000 processor.

representation is $\mathcal{G}^{R(A)} = 1/(\epsilon - \epsilon_{\mathcal{P}} \pm \mathrm{i}\frac{\hbar}{2\tau})$. The approximation

$$\frac{\hbar^2(-\mathcal{P}+\boldsymbol{q})^2}{2m} \approx \frac{\hbar^2\mathcal{P}^2}{2m} + \hbar v_F q$$

has also been used.

Appendix B. The 3D calculation of I_2 and the diffusion operator

The integral of the product of two Green's functions is needed to derive the diffusion operator. To include the $\mathcal{P}_y$ dependence of the electron lifetime by impurity scattering, we must perform the integral including the transverse momentum. Using $\epsilon = \epsilon_{\|} + \epsilon_{\perp}$, we obtain:

$$\begin{aligned}
I_2 &\equiv \int \frac{\mathrm{d}\mathcal{P}}{(2\pi\hbar)^3}\mathcal{G}^A(\boldsymbol{q}-\mathcal{P})\mathcal{G}^R(\mathcal{P}) \\
&= \int \frac{\mathrm{d}\mathcal{P}_{\|}}{(2\pi\hbar)^2}\int \frac{\mathrm{d}\mathcal{P}_y}{(2\pi\hbar)} \\
&\quad \times \frac{1}{\epsilon_{\|}+\epsilon_{\perp}-\epsilon_{\mathcal{P}}-\mathrm{i}\frac{\hbar}{2\tau(\mathcal{P}_y)}}\,\frac{1}{\epsilon_{\|}+\epsilon_{\perp}-\epsilon_{\mathcal{P}}+\hbar\omega-\hbar v_F q+\mathrm{i}\frac{\hbar}{2\tau(\mathcal{P}_y-q_y)}} \\
&= \int \frac{\mathrm{d}\mathcal{P}_y}{(2\pi\hbar)}\,2\pi\mathrm{i}\frac{N_{2D}(\epsilon-\epsilon_{\perp}+\mathrm{i}\frac{\hbar}{2\tau(\mathcal{P}_y)})}{\hbar\omega-\hbar v_F q+\mathrm{i}\frac{\hbar}{2}(\frac{1}{\tau(\mathcal{P}_y)}+\frac{1}{\tau(\mathcal{P}_y-q_y)})} \\
&\approx \frac{\mathrm{i}}{\hbar}\int \mathrm{d}\mathcal{P}_y \frac{N_{2D}(\epsilon-\epsilon_{\perp})}{\omega-v_F q+\frac{\mathrm{i}}{2}(\frac{1}{\tau(\mathcal{P}_y)}+\frac{1}{\tau(\mathcal{P}_y-q_y)})}.
\end{aligned}$$

In the limits of small ω and q, we expand this equation as a series to obtain

$$\begin{aligned}
I_2 &= \frac{\mathrm{i}}{\hbar}\int \mathrm{d}\mathcal{P}_y N_{2D}(\epsilon-\epsilon_{\perp})\left[\frac{1}{\frac{\mathrm{i}}{2}(\frac{1}{\tau(\mathcal{P}_y)}+\frac{1}{\tau(\mathcal{P}_y-q_y)})}\,\frac{1}{1+\frac{2(\omega-v_F q)}{\mathrm{i}(\frac{1}{\tau(\mathcal{P}_y)}+\frac{1}{\tau(\mathcal{P}_y-q_y)})}}\right] \\
&= \frac{2}{\hbar}\int \mathrm{d}\mathcal{P}_y N_{2D}(\epsilon-\epsilon_{\perp})\frac{\tau(\mathcal{P}_y)\tau(\mathcal{P}_y-q_y)}{\tau(\mathcal{P}_y)+\tau(\mathcal{P}_y-q_y)} \\
&\quad \times\left[1-\frac{2(\omega-v_F q)\tau(\mathcal{P}_y)\tau(\mathcal{P}_y-q_y)}{\mathrm{i}(\tau(\mathcal{P}_y)+\tau(\mathcal{P}_y-q_y))}\right. \\
&\quad \left.-\frac{4(\omega-v_F q)^2(\tau(\mathcal{P}_y)\tau(\mathcal{P}_y-q_y))^2}{(\tau(\mathcal{P}_y)+\tau(\mathcal{P}_y-q_y))^2}+\cdots\right].
\end{aligned}$$

Noting that the transfer q_y is very small, we let $\tau(\mathcal{P}_y - q_y) = \tau(\mathcal{P}_y) - \alpha(\mathcal{P}_y)q_y$ where

$$\alpha(\mathcal{P}_y) \equiv \frac{\partial\tau(\mathcal{P}_y-q_y)}{\partial\mathcal{P}_y}|_{q_y=0}.$$

We obtain

$$\begin{aligned}
I_2 &= \frac{2}{\hbar}\int \mathrm{d}\mathcal{P}_y N_{2D}(\epsilon-\epsilon_{\perp})\frac{\tau(\mathcal{P}_y)[\tau(\mathcal{P}_y)-\alpha(\mathcal{P}_y)q_y]}{2\tau(\mathcal{P}_y)-\alpha(\mathcal{P}_y)q_y} \\
&\quad \times\left[1-\frac{2(\omega-v_F q)\tau(\mathcal{P}_y)[\tau(\mathcal{P}_y)-\alpha(\mathcal{P}_y)q_y]}{\mathrm{i}(2\tau(\mathcal{P}_y)-\alpha(\mathcal{P}_y)q_y)}\right. \\
&\quad \left.-\frac{4(\omega-v_F q)^2[\tau(\mathcal{P}_y)(\tau(\mathcal{P}_y)-\alpha(\mathcal{P}_y)q_y)]^2}{(2\tau(\mathcal{P}_y)-\alpha(\mathcal{P}_y)q_y)^2}+\cdots\right].
\end{aligned}$$

Expanding this expression in q_y, again up to second order, we notice that:

$$\frac{1}{2\tau(\mathcal{P}_y)-\alpha(\mathcal{P}_y)q_y}=\frac{1}{2\tau(\mathcal{P}_y)}\frac{1}{1-\frac{\alpha(\mathcal{P}_y)q_y}{2\tau(\mathcal{P}_y)}}$$
$$\approx\frac{1}{2\tau(\mathcal{P}_y)}\left[1+\frac{\alpha(\mathcal{P}_y)q_y}{2\tau(\mathcal{P}_y)}+\frac{(\alpha(\mathcal{P}_y))^2q_y^2}{4(\tau(\mathcal{P}_y))^2}\right]$$

$$\frac{1}{(2\tau(\mathcal{P}_y)-\alpha(\mathcal{P}_y)q_y)^2}\approx\frac{1}{4(\tau(\mathcal{P}_y))^2}\left[1+\frac{\alpha(\mathcal{P}_y)q_y}{\tau(\mathcal{P}_y)}+\frac{3(\alpha(\mathcal{P}_y))^2q_y^2}{2(\tau(\mathcal{P}_y))^2}\right].$$

Hence, we obtain

$$I_2=\frac{2}{h}\int \mathrm{d}\mathcal{P}_y N_{2D}(\epsilon-\epsilon_\perp)\tau(\mathcal{P}_y)[\tau(\mathcal{P}_y)-\alpha(\mathcal{P}_y)q_y)]\frac{1}{2\tau(\mathcal{P}_y)}$$
$$\times\left[1+\frac{\alpha(\mathcal{P}_y)q_y}{2\tau(\mathcal{P}_y)}+\frac{(\alpha(\mathcal{P}_y))^2q_y^2}{4(\tau(\mathcal{P}_y))^2}\right]\left[1+\mathrm{i}2(\omega-v_Fq)\tau(\mathcal{P}_y)\right.$$
$$\times[\tau(\mathcal{P}_y)-\alpha(\mathcal{P}_y)q_y)]\frac{1}{2\tau(\mathcal{P}_y)}\left[1+\frac{\alpha(\mathcal{P}_y)q_y}{2\tau(\mathcal{P}_y)}+\frac{(\alpha(\mathcal{P}_y))^2q_y^2}{4(\tau(\mathcal{P}_y))^2}\right]$$
$$-4(\omega-v_Fq)^2[\tau(\mathcal{P}_y)(\tau(\mathcal{P}_y)-\alpha(\mathcal{P}_y)q_y)]^2\frac{1}{2(\tau(\mathcal{P}_y))^2}$$
$$\left.\times\left[1+\frac{\alpha(\mathcal{P}_y)q_y}{\tau(\mathcal{P}_y)}+\frac{3(\alpha(\mathcal{P}_y))^2q_y^2}{2(\tau(\mathcal{P}_y))^2}\right]\right].$$

Using the approximation $(\omega-v_Fq)^2\sim v_F^2q^2$ in the small ω limit we find

$$I_2=\frac{1}{h}\int \mathrm{d}\mathcal{P}_y N_{2D}(\epsilon-\epsilon_\perp)\left[\tau(\mathcal{P}_y)\left[1+\mathrm{i}\omega\tau(\mathcal{P}_y)+\mathrm{i}v_F\alpha(\mathcal{P}_y)q_y\left[q+\frac{\mathrm{i}}{2v_F\tau(\mathcal{P}_y)}\right]\right.\right.$$
$$\left.\left.-v_F^2(\tau(\mathcal{P}_y))^2\left[q+\frac{\mathrm{i}}{2v_F\tau(\mathcal{P}_y)}\right]^2-\frac{1}{4}\right]-\frac{(\alpha(\mathcal{P}_y))^2q_y^2}{4\tau(\mathcal{P}_y)}\right].$$

Unfortunately, the above result is so complicated that it leads to an unsolvable diffusion operator. Thus approximations are needed. We compare the magnitude of q with $1/2v_F\tau(\mathcal{P}_y)$, and since $1/\tau(\mathcal{P}_y)\sim u^2n_i/\hbar\epsilon_F$, we have

$$\frac{1}{2v_F\tau(\mathcal{P}_y)}\sim\frac{u^2n_i\mathcal{P}_F}{4\hbar\epsilon^2}\sim\left[\frac{u}{\epsilon_F}\right]^2\frac{n_i\pi}{4W}.$$

On the other hand $q\sim\pi/L$, so that

$$\frac{\frac{1}{2v_F\tau(\mathcal{P}_y)}}{q}\sim\left[\frac{u}{\epsilon_F}\right]^2\frac{n_iL}{4W}.$$

Furthermore, we have $L\sim W$, and $u\ll\epsilon_F$ (which is the important condition for the use of perturbation theory). Hence we conclude that

$$\frac{1}{2v_F\tau(\mathcal{P}_y)}\ll q$$

and simplify the integral I_2:

$$I_2=\frac{1}{h}\int \mathrm{d}\mathcal{P}_y N_{2D}(\epsilon-\epsilon_\perp)\left[\tau(\mathcal{P}_y)\left[\frac{3}{4}+\mathrm{i}\omega\tau(\mathcal{P}_y)+\mathrm{i}v_F\alpha(\mathcal{P}_y)q_yq-v_F^2(\tau(\mathcal{P}_y))^2q^2\right]\right.$$
$$\left.-\frac{(\alpha(\mathcal{P}_y))^2q_y^2}{4\tau(\mathcal{P}_y)}\right]. \tag{26}$$

To simplify the notation we define the following functions

$$\Gamma^{(1)} \equiv \frac{1}{\hbar}\int \mathrm{d}\mathcal{P}_y N_{2D}(\epsilon-\epsilon_\perp)\tau(\mathcal{P}_y)$$
$$\Gamma^{(2)} \equiv \frac{1}{\hbar^2}\int \mathrm{d}\mathcal{P}_y N_{2D}(\epsilon-\epsilon_\perp)(\tau(\mathcal{P}_y))^2$$
$$\Gamma^{(3)} \equiv \frac{1}{\hbar}\int \mathrm{d}\mathcal{P}_y N_{2D}(\epsilon-\epsilon_\perp)(\tau(\mathcal{P}_y))^3$$
$$\Gamma^{(4)} \equiv \frac{1}{\hbar}\int \mathrm{d}\mathcal{P}_y N_{2D}(\epsilon-\epsilon_\perp)\tau(\mathcal{P}_y)\alpha(\mathcal{P}_y)$$
$$\Gamma^{(5)} \equiv \frac{1}{\hbar}\int \mathrm{d}\mathcal{P}_y N_{2D}(\epsilon-\epsilon_\perp)\frac{(\alpha(\mathcal{P}_y))^2}{\tau(\mathcal{P}_y)} \tag{27}$$

and note that

$$\alpha(\mathcal{P}_y) = \frac{\partial\tau(\mathcal{P}_y - q_y)}{\partial\mathcal{P}_y}|_{q_y=0}.$$

With these definitions we rewrite (26) as

$$I_2 = \frac{3}{4}\Gamma^{(1)} + \mathrm{i}\omega\Gamma^{(2)} - \frac{1}{3}v_F^2\Gamma^{(3)}q^2 + \mathrm{i}v_F\Gamma^{(4)}q_y q - \frac{1}{4}\Gamma^{(5)}q_y^2. \tag{28}$$

Finally we mention that for the sake of simplicity we had written $v_F q$ instead of the vector expression $\boldsymbol{v}_F \cdot \boldsymbol{q}$. In the final expression of (28) there is therefore an additional $\frac{1}{3}$ factor.

In momentum representation the diffusion operator now becomes $[1 - u^2 n_i I_2]/u^2 n_i$. This we write in momentum representation as

$$\frac{1}{u^2 n_i} - \frac{3}{4}\Gamma^{(1)} - \mathrm{i}\omega\Gamma^{(2)} + \frac{1}{3}v_F^2\Gamma^{(3)}q^2 - \mathrm{i}v_F\Gamma^{(4)}q_y q + \frac{1}{4}\Gamma^{(5)}q_y^2$$

with a corresponding real space expression

$$\frac{1}{u^2 n_i} - \frac{3}{4}\Gamma^{(1)} - \mathrm{i}\omega\Gamma^{(2)} - \frac{1}{3}v_F^2\Gamma^{(3)}\nabla^2 + \mathrm{i}v_F\Gamma^{(4)}\frac{\partial}{\partial y}\left(\frac{\partial}{\partial x} + \frac{\partial}{\partial y} + \frac{\partial}{\partial z}\right) - \frac{1}{4}\Gamma^{(5)}\frac{\partial^2}{\partial y^2}. \tag{29}$$

Appendix C. The 2D expressions

For two spatial dimensions, the calculation procedures for I_1 and I_2 of equations (25) and (26) are the same as in the 3D case. However, the following trivial changes are required. First, the total electron lifetime is given by (10). Second, the 2D density of states $N_{2D}(\epsilon-\epsilon_\perp)$ is replaced by the one-dimensional (1D) density of states $N_{1D}(\epsilon-\epsilon_\perp)$ in the integrals I_1 and I_2. Finally the factor before the term with v_F^2 in I_2 changes from $\frac{1}{3}$ to $\frac{1}{2}$.

With these changes, we rewrite the definitions of the Γ functions of (27) in 2D:

$$\Gamma^{(1)} \equiv \frac{1}{\hbar}\int \mathrm{d}\mathcal{P}_y N_{1D}(\epsilon-\epsilon_\perp)\tau(\mathcal{P}_y)$$
$$\Gamma^{(2)} \equiv \frac{1}{\hbar^2}\int \mathrm{d}\mathcal{P}_y N_{1D}(\epsilon-\epsilon_\perp)(\tau(\mathcal{P}_y))^2$$
$$\Gamma^{(3)} \equiv \frac{1}{\hbar}\int \mathrm{d}\mathcal{P}_y N_{1D}(\epsilon-\epsilon_\perp)(\tau(\mathcal{P}_y))^3$$
$$\Gamma^{(4)} \equiv \frac{1}{\hbar}\int \mathrm{d}\mathcal{P}_y N_{1D}(\epsilon-\epsilon_\perp)\tau(\mathcal{P}_y)\alpha(\mathcal{P}_y)$$
$$\Gamma^{(5)} \equiv \frac{1}{\hbar}\int \mathrm{d}\mathcal{P}_y N_{1D}(\epsilon-\epsilon_\perp)\frac{(\alpha(\mathcal{P}_y))^2}{\tau(\mathcal{P}_y)}. \tag{30}$$

Furthermore we define the following quantities,

$$\begin{aligned}
\boldsymbol{C}_0 &\equiv 1 - u^2 n_i \left[\frac{3}{4}\Gamma^{(1)} + \mathrm{i}\omega\Gamma^{(2)}\right] \\
\boldsymbol{C}_1 &\equiv -\frac{1}{2}u^2 n_i v_F^2 \Gamma^{(3)} \\
\boldsymbol{C}_2 &\equiv -u^2 n_i \left[\frac{1}{2}v_F^2\Gamma^{(3)} - \mathrm{i}v_F\Gamma^{(4)} + \frac{1}{4}\Gamma^{(5)}\right] \\
\boldsymbol{C}_3 &\equiv \mathrm{i}u^2 n_i v_F \Gamma^{(4)}.
\end{aligned} \tag{31}$$

The real space diffusion operator in 2D then becomes

$$\left[\boldsymbol{C}_0 + \boldsymbol{C}_1\frac{\partial^2}{\partial x^2} + \boldsymbol{C}_2\frac{\partial^2}{\partial y^2} + \boldsymbol{C}_3\frac{\partial^2}{\partial x\partial y}\right] \tag{32}$$

where $\boldsymbol{x} = (x, y)$ is a 2D coordinate vector. We assume that in two dimensions the direction of electron transport is along the x-axis.

Appendix D. The anisotropic eigenvalue equation

To solve (13) we use a coordinate transformation:

$$x' = a_{11}x + a_{12}y \tag{33}$$

$$y' = a_{21}x + a_{22}y \tag{34}$$

Substituting (33) and (34) into (13) and adjusting a_{ij} such that:

$$\boldsymbol{C}_1 a_{11}^2 + \boldsymbol{C}_2 a_{12}^2 + \boldsymbol{C}_3 a_{11}a_{12} = 0 \tag{35}$$

$$\boldsymbol{C}_1 a_{21}^2 + \boldsymbol{C}_2 a_{22}^2 + \boldsymbol{C}_3 a_{21}a_{22} = 0. \tag{36}$$

yields

$$\left[\boldsymbol{C}_0 + (2\boldsymbol{C}_1 a_{11}a_{21} + 2\boldsymbol{C}_2 a_{12}a_{22} + \mathbf{C}_3 a_{11}a_{22} + \boldsymbol{C}_3 a_{21}a_{12})\frac{\partial^2}{\partial x'\partial y'}\right]\boldsymbol{Q}_m(\boldsymbol{x}') = \lambda_m \boldsymbol{Q}_m(\boldsymbol{x}'). \tag{37}$$

When $2\boldsymbol{C}_1 a_{11}a_{21} + 2\boldsymbol{C}_2 a_{12}a_{22} + \boldsymbol{C}_3 a_{11}a_{22} + \boldsymbol{C}_3 a_{21}a_{12} \neq 0$, we define the parameter c as

$$c \equiv \frac{4[\boldsymbol{C}_0 - \lambda_m]}{2\boldsymbol{C}_1 a_{11}a_{21} + 2\boldsymbol{C}_2 a_{12}a_{22} + \boldsymbol{C}_3 a_{11}a_{22} + \boldsymbol{C}_3 a_{21}a_{12}} \tag{38}$$

so that (37) becomes an equation of standard Riemannian form:

$$\left[\frac{\partial^2}{\partial x'\partial y'} + \frac{1}{4}c\right]\boldsymbol{Q}_m(x', y') = 0. \tag{39}$$

To solve this equation, we make a further nonlinear transform,

$$\kappa(x, y) \equiv \sqrt{c(x' - x_0)(y' - y_0)} \tag{40}$$

which transforms the Riemannian equation (39) into the zeroth-order Bessel equation:

$$\frac{\partial^2 \boldsymbol{Q}_m(\kappa)}{\partial \kappa^2} + \frac{1}{\kappa}\frac{\partial \boldsymbol{Q}_m(\kappa)}{\partial \kappa} + \boldsymbol{Q}_m(\kappa) = 0.$$

We thus obtain its solution $\boldsymbol{Q}(\boldsymbol{x})$ as

$$\boldsymbol{Q}(\boldsymbol{x}') = J_0(\sqrt{c(x' - x_0)(y' - y_0)})$$

where x_0 and y_0 are two arbitrary constants which will, without loss of generality, be put to zero. Finally, restoring the original variables from (33)–(34), we find the solution of (13) to be:

$$\boldsymbol{Q}_m(\boldsymbol{x}) = J_0(\sqrt{c(a_{11}x + a_{12}y)(a_{21}x + a_{22}y)}). \tag{41}$$

The constants $\{a_{ij}\}$ and the complex constant c which give the eigenvalues are determined by the relevant boundary conditions of the sample. We assume the same environment as that discussed in [25]: the sample is in contact with an insulator on the boundaries $y = y_1$ and $y = y_2$ so that no current flows normal to these boundaries. In addition we assume that in the direction of the current flow, the boundaries are good metallic contacts. Hence:

$$\frac{\partial \boldsymbol{Q}_m(x, y)}{\partial y}|_{y=y_1, y=y_2} = 0 \tag{42}$$

$$\boldsymbol{Q}_m(x, y)|_{x=0, x=L} = 0. \tag{43}$$

Equation (42) determines the eigenvalues for the x-direction, and (43) those for the y-direction. From (42) we obtain

$$J_1(\sqrt{c(a_{11}x)(a_{21}x)}) = 0$$
$$J_1(\sqrt{c(a_{11}x + a_{12}W)(a_{21}x + a_{22}W)}) = 0.$$

Denoting the zeros of J_1 by $y_1^{(i)}(i = 1, 2, 3, \ldots)$ we then obtain

$$ca_{11}a_{21}x^2 = (y_1^{(i)})^2$$
$$c[a_{11}a_{21}x^2 + (a_{11}a_{22} + a_{12}a_{21})Wx + a_{12}a_{22}W^2] = (y_1^{(j)})^2$$

and derive the first equation determining the eigenvalues in the x-direction:

$$a_{11}a_{21}[(y_1^{(j)})^2 - (y_1^{(i)})^2 - ca_{12}a_{22}W^2]^2 = cW^2(a_{11}a_{22} + a_{12}a_{21})^2(y_1^{(i)})^2. \tag{44}$$

Together with (35)–(36) and the unitary transformation (33)–(34), this equation uniquely determines all the constants as well as the needed eigenvalues in the x-direction.

Similarly from (43), we have

$$J_0(\sqrt{c(a_{12}y)(a_{22}y)}) = 0$$
$$J_0(\sqrt{c(a_{11}L + a_{12}y)(a_{21}L + a_{22}y)}) = 0$$

and denoting the zeros of J_0 by $y_0^{(i)}(i = 1, 2, 3, \ldots)$ we then obtain

$$ca_{12}a_{22}y^2 = (y_0^{(i)})^2$$
$$c[a_{11}a_{21}L^2 + (a_{11}a_{22} + a_{12}a_{21})Ly + a_{12}a_{22}y^2] = (y_0^{(j)})^2.$$

The second equation, which determines the eigenvalues in the y-direction is thus:

$$a_{12}a_{22}[(y_0^{(j)})^2 - (y_0^{(i)})^2 - ca_{11}a_{21}L^2]^2 = cL^2(a_{11}a_{22} + a_{12}a_{21})^2(y_0^{(i)})^2. \tag{45}$$

If we let $y_1^{(i)} = y_1^{(j)}$ and $y_0^{(i)} = y_0^{(j)}$, we obtain only the trivial eigenvalues for (13), i.e. $\lambda_m \equiv \boldsymbol{C}_0$. We shall not consider this trivial case. However, the non-trivial eigenvalues are used for the computation of the vertex functions, as described in the main text.

References

[1] See, for example, the review
van Houten H and Beenakker C W J 1991 *Solid State Physics* vol. **44**, ed H Ehrenreich and D Turnbull (San Diego: Academic)
[2] Lee P A and Stone A D 1985 *Phys. Rev. Lett.* **55** 1622
[3] Al'tshuler B L 1985 *JETP Lett.* **41** 648
[4] Entin M V 1969 *Sov. Phys.–Solid State* **11** 781
[5] Cheng Y C 1971 *Surf. Sci.* **27** 663
Cheng Y C 1972 *J. Jpn. Soc. Appl. Phys. Suppl.* **41** 173
Cheng Y C 1973 *Surf. Sci.* **40** 433
Cheng Y C 1974 *Jpn. J. Appl. Phys. Suppl.* **2** 363
Cheng Y C and Sullivan E A 1973 *J. Appl. Phys.* **44** 923
Cheng Y C and Sullivan E A 1973 *J. Appl. Phys.* **44** 3619
Cheng Y C and Sullivan E A 1973 *Surf. Sci.* **34** 717
[6] Matsumoto Y and Uemura Y 1974 *Jpn. J. Appl. Phys. Suppl.* **2** 367
Ando T 1977 *J. Phys. Soc. Jpn.* **43** 1616
[7] Mori S 1979 *Phys. Rev.* B **19** 6433
[8] Krutsick T J, White M H, Wong Hon-Sum and Booth R V 1987 *IEEE Trans. Electron Devices* **34** 1676
[9] Yalabik M C, Neofotistos G, Diff K, Guo Hong and Gunton J D 1989 *IEEE Trans. Electron Devices* **36** 1009
[10] Bonnefoi R, Chow D H and McGill T C 1987 *J. Appl. Phys.* **62** 3836
Kirby S K, Ting D Z-Y and McGill T C 1993 *Phys. Rev.* B **48** 15237
[11] Hillmer H, Forchel A, Sauer R and Tu C W 1990 *Phys. Rev.* B **42** 3220
[12] Thornton T J, Roukes M L, Scherer A and Van de Gaag B P 1989 *Phys. Rev. Lett.* **63** 2128
[13] Fuchs K 1938 *Proc. Cambridge Phil. Soc.* **34** 100
[14] Maslov D L, Barnes C and Kirczenow G 1993 *Phys. Rev. Lett.* **70** 1984
Maslov D L, Barnes C and Kirczenow G 1993 *Phys. Rev.* B **48** 2543
[15] Akera H and Ando T 1991 *Phys. Rev.* B **43** 11676
[16] Ando T and Tamura H 1992 *Phys. Rev.* B **46** 2332
[17] Nikolic K and Mackinnon A 1994 *Phys. Rev.* B **50** 11008
[18] Harris R and Guo Hong 1995 *Phys. Rev.* B **51** 5491
[19] Zhu Ningjia, Guo Hong, and Harris R 1996 *Phys. Rev. Lett.* **77** 1825
[20] Landauer R 1957 *IBM J. Res. Dev.* **1** 223
Landauer R 1989 *J. Phys.: Condens. Matter* **1** 8099
[21] Chaplik A V and Entin M V 1969 *Sov. Phys.–JETP* **28** 514
[22] Colman D, Bate R T and Mize J P 1968 *J. Appl. Phys.* **39** 1923
[23] Jacob U, Vancea J and Hoffmann H 1990 *Phys. Rev.* B **41** 11852
[24] Doniach S and Sondheimer E H 1974 *Green's Functions for Solid State Physicists* (Massachusetts: Benjamin)
[25] Lee P A, Stone A D and Fukuyama H 1987 *Phys. Rev.* B **35** 1039
[26] Rammer J 1991 *Rev. Mod. Phys.* **63** 781
[27] Imry Y 1986 *Europhysics Lett.* **1** 249
Murat M, Gefen Y and Imry Y 1986 *Phys. Rev.* B **34** 659
[28] Gupta M S 1994 *IEEE Trans. Electron Devices* **41** 2093
[29] Thouless D J 1974 *Phys. Rep.* **13** 93
[30] Anderson P W and Lee P A 1980 *Prog. Theor. Phys. Suppl.* **69** 212
[31] Edwards J T and Thouless D J 1972 *J. Phys. C: Solid State Phys.* **5** 807
[32] Tamura H and Ando T 1991 *Phys. Rev.* B **44** 1792
[33] Lent C S 1990 *J. Appl. Phys.* **67** 6353
[34] Wang Y, Wang J and Guo H 1994 *Phys. Rev.* B **49** 1928